Performance Analysis of Photovoltaic/Battery Unit Voltage and Frequency Control in Islanded Microgrid Under Several Load Unbalances

Pedro A. de Alcântara * **Luana C. S. Soares** *
Lindemberg R. de Lima ** **Camila M. V. Barros** ***
Luciano S. Barros ***

* *Electrical Engineering Graduate Program, Federal University of Paraíba, PB, (e-mails: pedro.alcantra@cear.ufpb.br, luana.soares@cear.ufpb.br).*
** *Mathematics and Computational Modeling Graduate Program, Federal University of Paraíba, PB, (e-mail: lindemberg.roberto@academico.ufpb.br)*
*** *Computer Systems Department, Informatic Center, Federal University of Paraíba,PB, (e-mails: camila.barros@ci.ufpb.br, lsalesbarros@ci.ufpb.br)*

Abstract: The concept of autonomous microgrids has strongly increased due to the large penetration of distributed generation into the main grid, mainly photovoltaic systems. Attached to these generation units, Battery Energy Storage Systems (BESS) has been widely used to support voltage and frequency regulation since it provides a fast system response. Therefore, this microgrid configuration has extensively used a grid-forming droop control strategy in order to provide a frequency and voltage controlling interface for islanded operation mode. Although there are several studies in the literature proving that this strategy works properly, performance analyses under several load unbalances have been little addressed. This paper aims to analyze a photovoltaic/battery-based islanded microgrid architecture under the previously mentioned load scenario. The proposed work analysis has been performed through simulations using Matlab/Simulink from the modeling of all microgrid components. It was observed that in a low load power scenario, losses caused by more than 20% of unbalance degree cause BESS to not work properly, discharging instead of charging. With a high load power scenario, an unbalance degree of 45% is enough to make the system unable to control DC-Link voltage and consequently not keep AC voltage level.

Keywords: islanded microgrid, photovoltaic/battery unit, grid-forming control, droop control, unbalanced loads.

1. INTRODUCTION

Distributed generation in Brazil has been growing considerably in recent years. According to the Brazilian Electrical Energy National Agency (ANEEL, in Portuguese) and Brazilian Association of Distributed Generation (ABGD, in Portuguese), by January 2022 distributed generation (DG) units reached 10 GW of installed power, where 97.7% of these units are represented by photovoltaic (PV) generation systems (ABGD, 2022).

Energy storage systems, load, and the growth of local energy generation systems together form microgrids (MGs). This strong penetration of DG systems to the main grid makes MGs the target of studies and discussions. Therefore, studying MGs' capacity for operating grid-connected or in islanded mode has become crucial.

The literature includes some works on power management and load sharing in islanded-hybrid three/single-phase MGs. For example, in Mahmood et al. (2015), a hybrid islanded MG with droop control is proposed. The

control system allows the MG to adapt autonomously to the operating conditions by charging or discharging the battery and controlling the PV unit power. The work of Karimi et al. (2017) proposes a power control strategy and load sharing in a single/three-phase-islanded MG with hybrid source PV/battery units. In this work, the level of grid frequency is used to switch the operating state of the MG according to the conditions of the generation units. In another example, Sun et al. (2015) proposes a structure of hybrid MG using a control strategy based on single-phase back-to-back converters. In this work, the single-phase and three-phase generation units were controlled separately.

Although all these works are important, they do not comprehend all the evaluation possibilities of an MG's behavior and its control strategies under unbalanced loads. Works like Vijay et al. (2020) compare droop control combinations of distributed generators under some unbalanced load conditions. However, MG's behavior with traditional grid-forming droop control under several load unbalances is little addressed. Thus, this work aims to
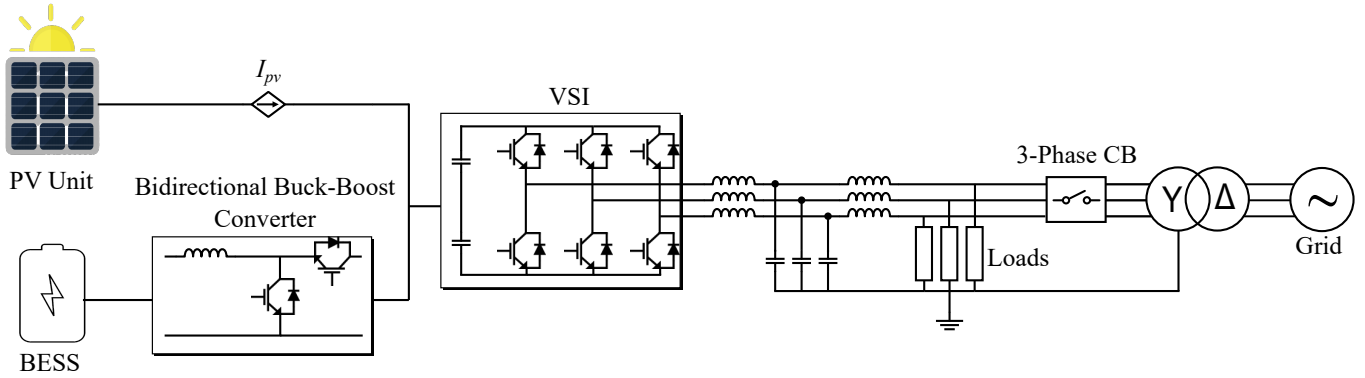
Figure 1. Microgrid architecture studied in this paper.

analyze an islanded-droop-controlled-three-phase MG architecture composed of a current-source-represented PV unit, and a Lithium-Ion Battery Energy Storage System (BESS), under several load unbalance levels.

The rest of the work is structured as follows: Section 2 is dedicated to detailing MG's elements and modeling. Section 3 describes the control systems, ranging from Voltage Source Inverter (VSI)'s grid-forming control to BESS's bidirectional DC-DC converter control. In Section 4, the results obtained from simulations in all MG evaluation scenarios are presented. Finally, Section 5 concludes the work.

2. MICROGRID DESCRIPTION AND MODELING

Figure 1 shows the MG configuration studied in this paper. It consists of a controlled current source (I_{pv}) used to represent the PV unit, a BESS, the VSI, and the loads. The BESS feeds the DC link through a bidirectional DC-DC converter, while the VSI is connected to the loads through an LCL filter (da Silva Junior et al., 2021), (Mahmood et al., 2012). A three-phase circuit breaker (CB) switches the system from grid-connected to islanded mode (Karimi et al., 2017).

This work used 47 $3.3V$ $LiFePO_4$ cells as a reference for modeling BESS. According to da Silva Junior et al. (2021), the model is based on the interpolation of data obtained in experimental tests made by Baronti et al. (2013), that relates the hysteresis between state-of-charge (SoC) and the battery open-circuit voltage (V_{oc}).

Depending on the MG load scenario, BESS needs to charge or discharge to keep the power balance. Therefore, a bidirectional buck-boost converter is needed. It operates in buck mode when BESS is in charge, and in boost mode when BESS is in discharge (de Matos et al., 2015).

3. CONTROL SYSTEMS

The focus of this work is to analyze the MG's control system when it is operating in islanded mode. However, as it will be shown in Section 4, the simulation starts grid-connected and then the CB switches it to islanded mode. Therefore, a VSI control system is provided to control DC link voltage (V_{dc}) when MG operates grid-connected. The control system used in this situation it's the same presented by Barros and Barros (2017) and it's
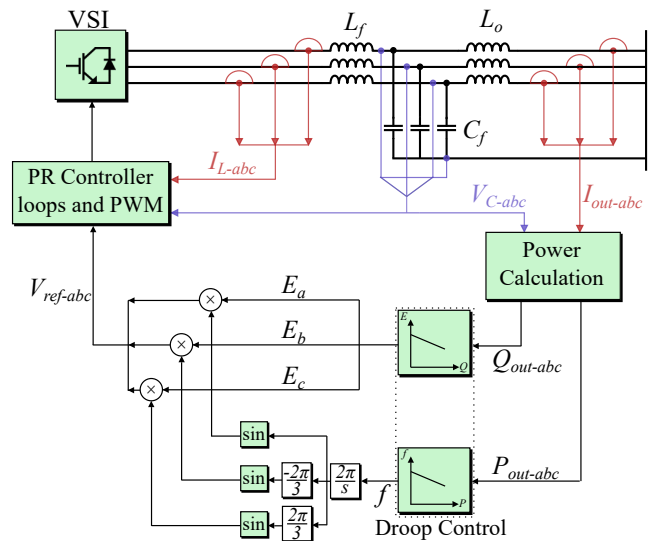

Figure 2. Grid-forming VSI control schematic for islanded operation mode. Adapted from Karimi et al. (2017).

not detailed here. It's also important to emphasize that islanding detection is beyond the scope of this paper.

Grid-forming VSI control strategy for islanded operation mode is depicted in Figure 2. Instantaneous active and reactive power are calculated according to Akagi et al. (1984). The droop control strategy is implemented as a decentralized control method for the VSI. This kind of control does not require communication between units, but only local measurements, increasing the reliability of the system. Proportional-Resonant (PR) controllers are attached to droop control to track the reference voltage through inner current and voltage loops in order to achieve zero steady-state error (Karimi et al., 2017). Finally, BESS bidirectional buck-boost converter control is implemented in order to regulate V_{dc} to a predefined value (V_{dc}^*). It is important to highlight the role of PV Maximum Power Point Tracker (MPPT) in maintaining the output power during the MG operation since in this work this considers an ideal current source to model the PV with MPPT. These control strategies are described in the following subsections.

3.1 Droop Control

According to the power transmission theory, once the inverter output impedance is mainly inductive, the tra-

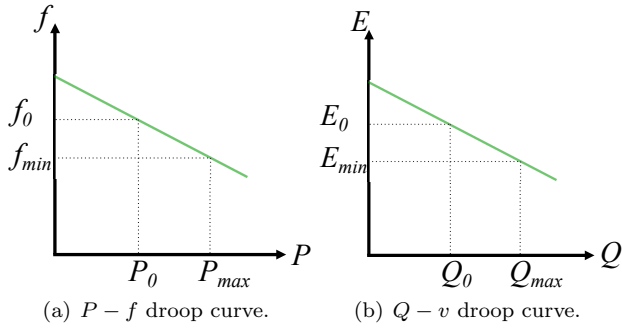(a) $P - f$ droop curve.   (b) $Q - v$ droop curve.

Figure 3. Droop control characteristic curves.

ditional droop control strategy provides frequency and voltage amplitude references which are influenced by active and reactive power variation, respectively (Karaki et al., 2019) (ZHANG et al., 2018). Characteristic droop equations are described as:

$$f = f_0 + m \cdot (P_0 - P), \quad (1)$$

$$E = E_0 + n \cdot (Q_0 - Q), \quad (2)$$

where,

- m and n are frequency and voltage droop coefficients, respectively;
- f and f_0 are output and nominal frequency, respectively;
- E and E_0 are output and nominal voltage amplitude, respectively;
- P_0 and Q_0 are nominal active and reactive powers, respectively;
- P and Q are measured active and reactive powers, respectively;

From Equations (1) and (2), the obtained characteristic droop control curves are presented in Figures 3(a) and 3(b), respectively.

3.2 PR Control Loops

This article used PR control loops based on a stationary reference frame. The voltage reference (frequency and amplitude) is generated by droop control functions in abc and transformed into $\alpha\beta$ through the well-known Clarke transformation. The control system includes voltage and current loops tuned not just at the fundamental frequency, but at the 5th, 7th, and 11th harmonics as well. The whole implemented strategy is well detailed in Vasquez et al. (2013). Figure 4 presents an overall vision of the control strategy.

3.3 Bidirectional buck-boost converter control

All steady-state equations and controller projects for the DC-DC bidirectional converter used in this work may be found in Mahmood et al. (2012). Note that the present paper does not consider the charge and discharge limits of BESS, so the simulations are restricted to a safe SoC values range. Figure 5 presents the converter schematic and control diagram.
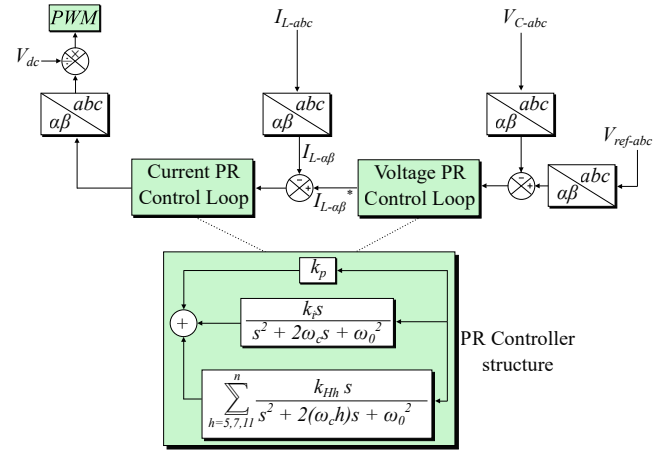

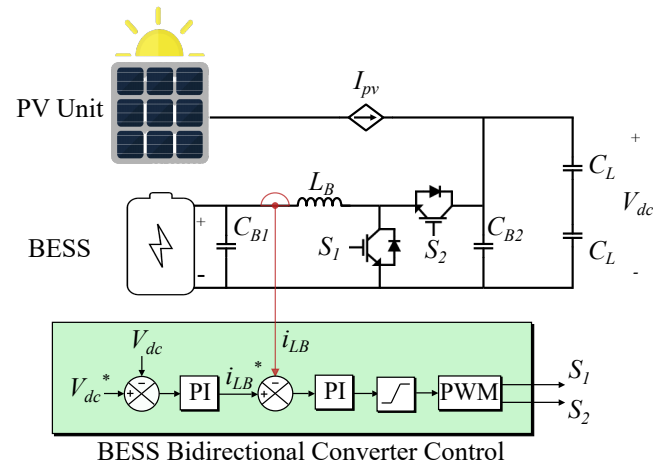Figure 4. PR Controller loops diagram. Adapted from Vasquez et al. (2013).

Figure 5. Bidirectional buck-boost converter schematic and control diagram.

4. SIMULATIONS AND RESULTS

The MG structure depicted in Figure 1 and the control systems described in Section 3 have been implemented using Matlab/Simulink. Table 1 lists the MG setup and all control parameters. As grid-connected mode is not detailed here, Table A.1 lists its control parameters.

Several simulations were performed in order to evaluate the MG behavior and control operational limits in the islanded mode under several load unbalance levels. Equations (3) and (4) were used to measure the load unbalance degree (K) (Wu et al., 2019):

$$K(\%) = \frac{max[|I_a - I_{avg}|, |I_b - I_{avg}|, |I_b - I_{avg}|]}{I_{avg}} \cdot 100, \quad (3)$$

$$I_{avg} = \frac{I_a + I_b + I_c}{3}, \quad (4)$$

where:

- I_a is the RMS load current of phase a;
- I_b is the RMS load current of phase b;
- I_c is the RMS load current of phase c;
- I_{avg} is the average RMS value of the three-phase load currents;

Table 1. Simulation setup and control parameters.

Parameter	Symbol	Value
DC-Link nominal voltage	V_{dc}	300V
Grid AC nominal voltage	V_g	$127V_{RMS}$
Nominal frequency	f_0	60Hz
PV Unit power	P_{pv}	1000W
BESS nominal voltage	V_{BESS}	155V
BESS capacity	C_{BESS}	20Ah
BESS converter inductance	L_B	10mH
BESS-side capacitance	C_{B1}	100μF
DC-Link-side capacitance	C_{B2}	38μF
DC-Link capacitances	C_L	500μF
VSI-side inductance	L_f	500μH
Grid-side inductance	L_o	500μH
Filter capacitance	C_f	9μF
BESS control voltage loop (PI)	K_{bpv}, K_{biv}	0.063, 150
BESS control current loop (PI)	K_{bpi}, K_{bii}	0.2325, 1.57
PR voltage loop	K_{pv}, K_{iv}	500, 500
PR current loop	K_{pi}, K_{ii}	100, 100
Frequency droop coefficient	m	0.005
Voltage droop coefficient	n	1

Additionally, root mean squared error (RMSE) calculations were performed to quantify the error among PR controller input reference voltage, provided by droop control, and the output load voltage waveform. Then, RMSE was calculated per phase as follows:

$$RMSE(\%) = \frac{1}{V_{ref}} \cdot \sqrt{\frac{1}{N} \sum_{i=1}^{N} (V_{ref} - V_g)^2} \cdot 100 \quad (5)$$

where:

- V_{ref} is the RMS reference voltage provided by droop control, per phase;
- V_g is the RMS load voltage per phase;
- N is the number of samples used;

It considers two main analysis scenarios:

- *Scenario 1*: the power provided by PV unit (P_{pv}) is 100% larger than the output load power (P_{out}), so the BESS absorb the surplus power;
- *Scenario 2*: P_{pv} is 33.3% smaller than P_{out}, so the BESS injects power to compensate the lack.

As aforementioned, simulations consider the transition from grid-connected to islanded mode. Until instant $1s$, the CB is switched on, and after that, it switches off to initiate islanded operation mode.

The simulation results for each scenario are presented in the following subsections.

4.1 Scenario 1

Since $P_{pv} > P_{out}$, V_{dc} tends to rise. BESS bidirectional converter controller detects V_{dc} variation and starts to operate as a buck, absorbing surplus power.

Droop control detects power variation in the MG. Since PV power is larger than load power, the frequency reference provided by droop control rises. As the loads considered in this work are represented by resistors, there is no output reactive power flowing in the system. For this reason, from Equation (2), the reference voltage amplitude is always at
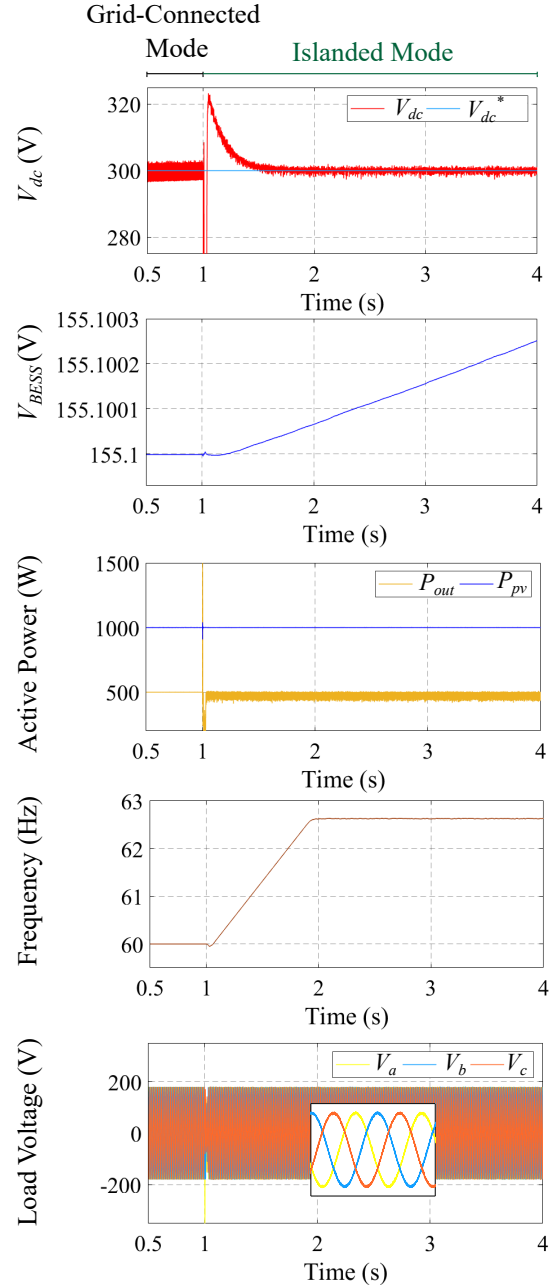

Figure 6. Simulation results of Scenario 1 for K=0%.

the nominal value, considering that the reference reactive power (Q_0) is zero.

Thus, the actual goal is to observe the MG control towards different degrees of load unbalances.

Simulations were performed by ranging K from 0% to 70%. It was observed that until 20% unbalance, the BESS bidirectional converter control performed as expected by operating in buck mode. However, for K values larger than 20%, due to the system power losses caused by load unbalance, BESS control tries to compensate it by discharging.

Another important point observed comprehends PR controller and droop control. For high load unbalance levels, the PR controller is not able to track voltage waveform. The calculation of RMSE was made per phase, and the

Table 2. RMSE per phase for Scenario 1.

-	RMSE[%]		
K [%]	Phase a	Phase b	Phase c
0	3.28	3.50	3.36
5	3.80	2.90	5.20
10	6.50	5.50	10.30
15	8.50	8.80	17.00
20	14.70	16.80	16.50
25	18.09	21.02	17.49
30	20.81	25.51	16.72
35	23.96	29.72	20.01
40	26.96	33.89	22.44
45	26.33	36.54	23.32
50	29.13	36.86	25.02
55	29.42	40.97	26.39
60	32.78	42.55	28.60
65	35.19	42.07	28.57
70	34.63	33.40	30.54

results are listed in Table 2. Note that the increase of K represents RMSE increase as well, proving that the PR controller was not able to avoid voltage distortions due to load unbalance. After 70% unbalance, the RMSE calculation is no longer accurate since the voltage reference provided by droop control is not correct.

To illustrate the aforementioned results, Figures 6 and 7 show graphically the simulation results for a balanced situation with $K=0\%$, and for a critical case with $K=70\%$, respectively.

In the first situation ($K=0\%$), it's possible to see that V_{dc} is controlled and BESS voltage (V_{BESS}) is rising, which means that BESS is controlling V_{dc} by charging, as expected. Grid frequency rises, proving droop control is working properly. Finally, load voltage waveforms are preserved thanks to the PR controller action.

In the second situation ($K=70\%$), there is a lot of distortion in V_{dc}, even though its mean value is preserved in $300V$. However, despite the low load power, V_{BESS} decreases, and it's possible to notice that the load voltage waveform is completely distorted, proving the PR controller's failure.

Once MG control systems work to maintain MG power balance, similar results are expected for any P_{pv}/P_{out} relation, since $P_{pv}>P_{out}$ condition and BESS limits are respected. However, it is important to highlight that the closer P_{out} is to P_{pv}, the K limit to proper MG operation decreases.

4.2 Scenario 2

Since $P_{pv}<P_{out}$, V_{dc} tends to decrease. This variation makes the BESS converter control system operate as a boost, and so provides the needed power.

In the same way, described for Scenario 1, droop control acts to provide the system voltage reference according to the grid power variations. In this case, frequency reference decreases. Again, the loads in this scenario are resistive, so reference voltage amplitude is nominal, considering $Q_0=0$.

For this scenario, K ranges from 0% to 45%. It was noticed that for $K>40\%$, the MG control system is not able to keep normal operation. There is a drop in V_{dc} and BESS is not able to supply the power lack caused by unbalance losses.
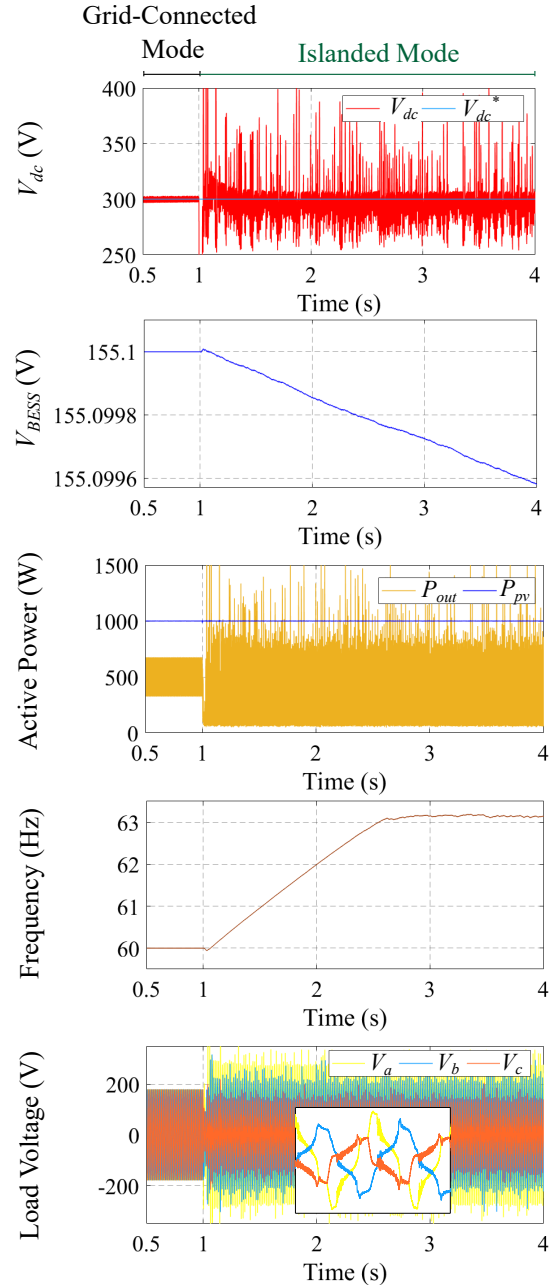

Figure 7. Simulation results of Scenario 1 for $K=70\%$.

Table 3. RMSE per phase for Scenario 2.

-	RMSE [%]		
K [%]	Phase a	Phase b	Phase c
0	8.34	8.95	7.64
5	18.49	8.39	14.91
10	22.46	12.73	21.19
15	33.07	15.65	26.43
20	39.44	18.78	30.38
25	45.94	22.49	33.87
30	49.00	24.24	36.43
35	50.25	29.66	39.34
40	31.4	32.03	41.05
45	0.08	18.48	24.30

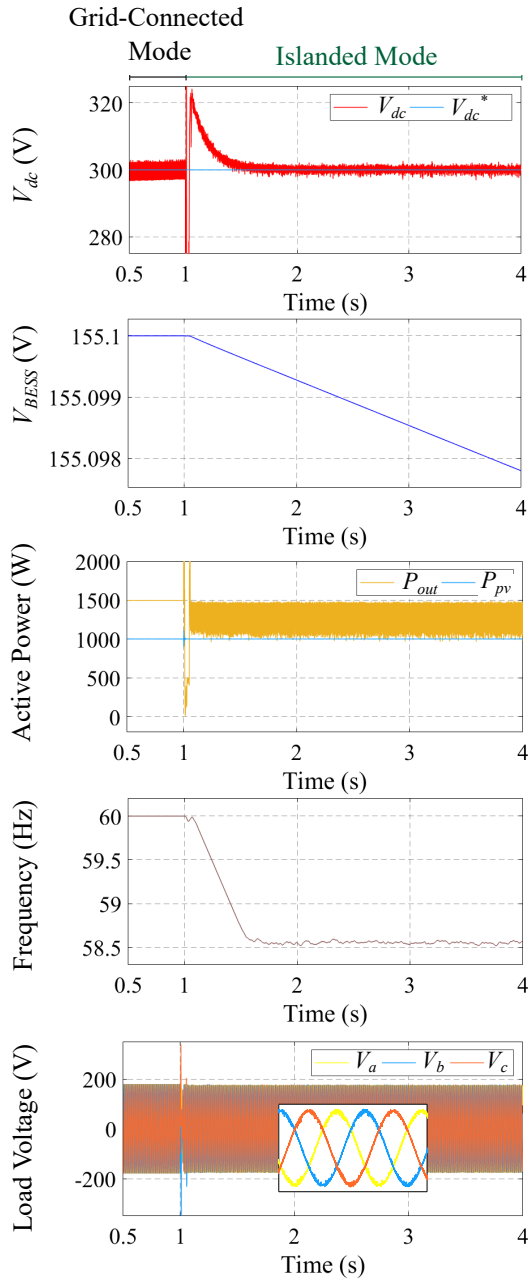Figure 8. Simulation results of Scenario 2 for $K = 0\%$.

Figure 9. Simulation results of Scenario 2 for $K=45\%$.

Calculation of RMSE was also performed as described in Scenario 1, and the results are listed in Table 3. Moreover, as K rises, RMSE per phase also rises. It is important to notice that after $K=40\%$, V_{dc} drops, and consequently P_{out} also drops. Again, the RMSE calculation for these cases is no longer accurate since droop control does not work properly. It confirms that the grid-forming control implemented is not able to operate under high load unbalance levels.

The aforementioned results are illustrated in Figures 8 and 9. A balanced situation ($K=0\%$) shows that the MG is operating properly. V_{BESS} discharges to compensate for the lack of power and control V_{dc}. As expected, MG frequency drops, since $P_{pv}<P_{out}$, proving once more that droop control works rightly.
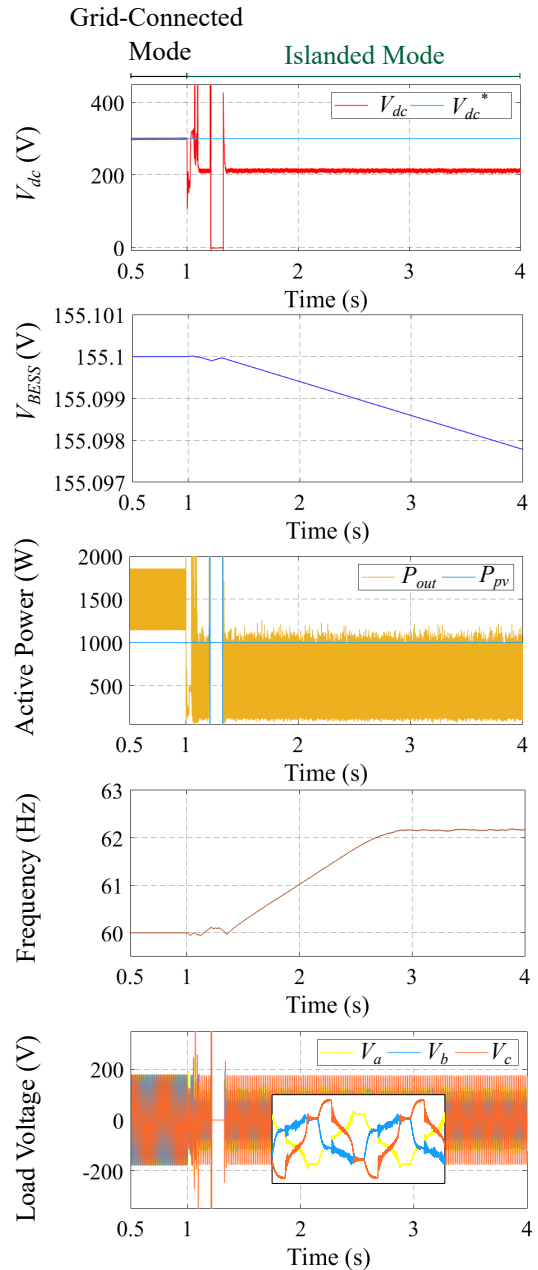
As mentioned for Scenario 1, similar results are waited for any P_{out}/P_{pv} relation, respecting $P_{pv}<P_{out}$ condition and BESS limits. Nevertheless, it is important to highlight that the larger P_{out} value, the smaller K limit to MG work properly.

5. CONCLUSION

This work modeled and simulated a three-phase-droop-controlled microgrid, composed of a photovoltaic-battery unit, and analyzed the control system behavior under several load unbalances. The analysis was performed in two different scenarios, considering the load power larger or smaller than photovoltaic power.

As result, it was observed that for larger photovoltaic power, unbalance levels above 20% provoke enough power losses to make BESS discharge instead charging. For

smaller photovoltaic power, an unbalance degree of 45% is enough to make the DC-link voltage drop, and consequently, load power also drops. In both scenarios, the high unbalance degree made grid-forming control unable to provide MG proper operation.

Appendix A. GRID-CONNECTED MODE CONTROL PARAMETERS AND LOAD DISTRIBUTIONS

Table A.1 lists control parameters used in grid-connected operation mode.

Table A.1. Grid-connected mode control parameters

Parameter	Symbol	Value
DC-link voltage loop (PI)	K_p, K_i	250, 500
Direct axis current loop (PI)	K_p, K_i	0.15, 0.5
Quadrature axis current loop (PI)	K_p, K_i	0.5, 0.15

Tables A.2 and A.3 list load distributions among phases, where R_a, R_b and R_c are load resistances of phase a, b and c, respectively.

Table A.2. Load distribution for Scenario 1.

-	Load distribution		
K [%]	$R_a[\Omega]$	$R_b[\Omega]$	$R_c[\Omega]$
0	96.80	96.80	96.80
5	100.80	97.80	92.80
10	93.80	108.20	90.10
15	95.70	114.00	84.90
20	121.00	96.80	80.60
25	129.00	94.90	78.70
30	138.40	87.90	80.60
35	149.30	88.60	76.80
40	161.30	85.80	76.10
45	176.30	83.40	75.00
50	196.70	82.70	72.30
55	218.00	80.0	71.40
60	244.40	76.80	72.00
65	278.10	76.10	70.10
70	322.60	73.30	70.10

Table A.3. Load distribution for Scenario 2.

-	Load distribution		
K [%]	$R_a[\Omega]$	$R_b[\Omega]$	$R_c[\Omega]$
0	32.30	32.30	32.30
5	30.70	32.30	34.00
10	29.30	33.60	34.30
15	29.10	31.00	38.00
20	27.80	31.00	40.30
25	26.90	30.70	43.00
30	26.00	30.40	46.10
35	25.60	29.60	49.60
40	24.80	29.30	53.80
45	23.70	29.60	58.70

ACKNOWLEDGEMENT

REFERENCES

ABGD, A.B.d.G.D. (2022). Brasil atinge 10 gw de potência instalada em sistemas de geração própria de energia. https://www.abgd.com.br/portal/blog-pg/161/brasil-atinge-10-gw-de-potencia-instalada-em-sistemas-de-geracao-propria-de-energia/. Accessed in: 18/04/2022.

Akagi, H., Kanazawa, Y., and Nabae, A. (1984). Instantaneous reactive power compensators comprising switching devices without energy storage components. *IEEE Transactions on Industry Applications*, IA-20(3), 625–630. doi:10.1109/TIA.1984.4504460.

Baronti, F., Zamboni, W., Femia, N., Roncella, R., and Saletti, R. (2013). Experimental analysis of open-circuit voltage hysteresis in lithium-iron-phosphate batteries. In *IECON 2013-39th Annual Conference of the IEEE Industrial Electronics Society*, 6728–6733. IEEE.

Barros, L.S. and Barros, C.M.V. (2017). Modificação no controle do lado da rede de geradores eólicos baseados em pmsg para ampliar a suportabilidade a afundamentos de tensão. *Eletrônica de Potência*, 22(2), 167–178.

da Silva Junior, G.P., Barros, L.S., and Barros, C.M.V. (2021). Synchronverter coupled to a lithium-ion bank for grid frequency and voltage supports and controlled charge-discharge. *Electric Power Systems Research*, 197, 107352.

de Matos, J.G., e Silva, F.S.F., and Ribeiro, L.A.d.S. (2015). Power control in ac isolated microgrids with renewable energy sources and energy storage systems. *IEEE Transactions on Industrial Electronics*, 62(6), 3490–3498. doi:10.1109/TIE.2014.2367463.

Karaki, A., Begovic, M., Bayhan, S., and Abu-Rub, H. (2019). Frequency and voltage restoration for droop controlled ac microgrids. In *2019 2nd International Conference on Smart Grid and Renewable Energy (SGRE)*, 1–6. doi:10.1109/SGRE46976.2019.9020914.

Karimi, Y., Oraee, H., and Guerrero, J.M. (2017). Decentralized method for load sharing and power management in a hybrid single/three-phase-islanded microgrid consisting of hybrid source pv/battery units. *IEEE Transactions on Power Electronics*, 32(8), 6135–6144. doi:10.1109/TPEL.2016.2620258.

Mahmood, H., Michaelson, D., and Jiang, J. (2012). Control strategy for a standalone pv/battery hybrid system. In *IECON 2012 - 38th Annual Conference on IEEE Industrial Electronics Society*, 3412–3418. doi:10.1109/IECON.2012.6389351.

Mahmood, H., Michaelson, D., and Jiang, J. (2015). Decentralized power management of a pv/battery hybrid unit in a droop-controlled islanded microgrid. *IEEE Transactions on Power Electronics*, 30(12), 7215–7229. doi:10.1109/TPEL.2015.2394351.

Sun, Q., Zhou, J., Guerrero, J.M., and Zhang, H. (2015). Hybrid three-phase/single-phase microgrid architecture with power management capabilities. *IEEE Transactions on Power Electronics*, 30(10), 5964–5977. doi:10.1109/TPEL.2014.2379925.

Vasquez, J.C., Guerrero, J.M., Savaghebi, M., Eloy-Garcia, J., and Teodorescu, R. (2013). Modeling, analysis, and design of stationary-reference-frame droop-controlled parallel three-phase voltage source inverters. *IEEE Transactions on Industrial Electronics*, 60(4), 1271–1280. doi:10.1109/TIE.2012.2194951.

Vijay, A.S., Parth, N., Doolla, S., and Chandorkar, M.C. (2020). Performance of droop controller combinations in islanded microgrids with unbalanced loads. In *2020 IEEE International Conference on Power Electronics, Drives and Energy Systems (PEDES)*, 1–5. doi:10.1109/PEDES49360.2020.9379562.

Wu, X., Li, J., Pang, W., and Chen, J. (2019). Research on improvement of line loss algorithm based on three-phase unbalance degree. In *2019 4th International Conference on Intelligent Green Building and Smart Grid (IGBSG)*, 563–566. doi:10.1109/IGBSG.2019.8886242.

ZHANG, H., GAO, Y., and LU, D. (2018). Micro-grid droop control strategy optimization and simulation. In *2018 China International Conference on Electricity Distribution (CICED)*, 2013–2017. doi:10.1109/CICED.2018.8592279.